npj | parkinson's disease

Article

Published in partnership with the Parkinson's Foundation

https://doi.org/10.1038/s41531-025-00971-8

Choroid plexus enlargement contributes to motor severity via regional glymphatic dysfunction in Parkinson's disease

Linyu Liu[1], Qiang Weng[2], Qing Cai[1], Xintong Yu[1], Weibin Huang[1], Shaohua Xie[3], Yan Shi[1], Huiting Li[1], Yuxuan Zhang[1], Jianping Hu[2], Mengcheng Li[2], Guannan Chen[4], Ning Wang[1] ✉, Xiang Lin[1] ✉, Ying Fu[1] ✉ & Yu Lin[1] ✉

Choroid plexus (CP) enlargement and glymphatic dysfunction have been implicated in neurodegeneration, but their roles in Parkinson's disease (PD) remain unclear. This retrospective cross-sectional study examined associations among CP volume, perivascular spaces (PVS), and motor symptom severity in 123 PD patients stratified by disease stage. MRI quantified CP volume and PVS, including dilated PVS (dPVS), across brain regions. CP-dPVS correlations were stronger in early-stage PD. Region-specific analyses revealed CP volume was associated with PVS in the midbrain and basal ganglia. CP-dPVS correlations emerged in midbrain, basal ganglia, and centrum semiovale. Correlation matrix and mediation analyses together confirmed that only basal ganglia dPVS was both significantly correlated with motor symptoms and served as a mediator, accounting for 30.52% of the association between CP volume and motor severity. These findings suggest that CP enlargement contributes to motor severity in PD, in part through regional glymphatic dysfunction localized to the basal ganglia.

Parkinson's disease (PD), the second most common neurodegenerative disorder, is characterized by progressive degeneration of dopaminergic neurons and the accumulation of misfolded α-synuclein, which drive the onset and progression of motor symptoms[1,2]. Emerging evidence highlights the critical role of cerebrospinal fluid (CSF) circulation in the accumulation and clearance of pathological proteins[3,4].

The CSF circulation system has two primary components: the choroid plexus (CP), which produces CSF, and the glymphatic system, which facilitates the drainage of interstitial fluid and waste[5]. Notably, CSF production and glymphatic clearance rates peak during sleep, suggesting a coordinated mechanism for waste removal[6,7]. In neurodegenerative diseases, alterations in CP function often occur alongside glymphatic impairment, indicating potential interactions between these systems. CP volume enlargement, which reflects changes in CSF production, has been associated with glymphatic dysfunction and the accumulation of pathological proteins in conditions such as Alzheimer's disease[8]. Previous studies propose that the CP may act as a pathway for α-synuclein clearance from the brain[9]. Furthermore, CP enlargement has been linked to reduced dopaminergic uptake, potentially exacerbating motor symptoms[10]. Similarly, dilated perivascular spaces (dPVS), a marker of glymphatic dysfunction, correlate with disease severity in PD[11,12]. Despite these findings, the precise relationship between CP alterations and PVS dynamics in PD, as well as their combined influence on motor symptom severity, remains poorly understood.

PD is characterized by substantial temporal and spatial heterogeneity, with neurodegenerative changes affecting distinct brain regions at different disease stages. This progression is thought to reflect α-synuclein aggregation, which follows a predictable pattern of increasing involvement of widespread brain regions and progressive accumulation across affected areas[13]. Evidence suggests that impaired protein clearance mechanisms, rather than solely increased α-synuclein production, play a critical role in its aggregation and accumulation in PD[14]. In particular, alterations in CP volume and PVS characteristics have been associated with defective α-synuclein clearance as the disease advances[9,15]. Therefore, understanding how CP volume and PVS dynamics evolve over time and across brain regions is essential for elucidating their roles in PD pathology.

[1]Department of Neurology, First Affiliated Hospital, Fujian Medical University, Fuzhou, Fujian, China. [2]Department of Radiology of First Affiliated Hospital, Fujian Medical University, Fuzhou, Fujian, China. [3]Department of Molecular Medicine and Surgery, Karolinska Institutet, Stockholm, Sweden. [4]Key Laboratory of OptoElectronic Science and Technology for Medicine of Ministry of Education, Fujian Provincial Key Laboratory of Photonics Technology, Fujian Normal University, Fuzhou, Fujian, China. ✉e-mail: ningwang@fjmu.edu.cn; linxiang1988@fjmu.edu.cn; fuying@fjmu.edu.cn; yulinwin2009@aliyun.com

In this study, we aimed to investigate the relationship between CP alterations and PVS dynamics in PD patients, focusing on their potential contributions to motor symptom severity. Specifically, we addressed the following questions: (i) Does the relationship between CP volume and PVS/dPVS change across early- and advanced-stage PD, reflecting temporal changes in disease pathology? (ii) How does CP volume correlate with PVS/dPVS characteristics in different brain regions? (iii) What do these findings imply for understanding motor symptom severity in PD?

Results

Demographic and MRI features

A total of 140 patients were initially enrolled in the study. After excluding 10 patients with parkinsonism due to other etiologies, 5 with incomplete clinical data, and 2 unable to undergo MRI due to claustrophobia, the final cohort consisted of 123 patients with PD (Fig. 1a). Demographic and MRI characteristics of the participants are summarized in Table 1.

Stage-specific associations between CP volume and PVS/dPVS

Partial correlation analysis revealed significant positive correlations between CP volume and total PVS/dPVS counts. Specifically, CP volume showed a positive correlation with PVS ($r = 0.358$, $p < 0.001$) and with dPVS counts ($r = 0.386$, $p < 0.001$, Fig. 2a, d). In both early- and advanced-stage groups, CP volume correlated positively with total PVS counts (early-stage: $r = 0.397$, $p = 0.002$; advanced-stage: $r = 0.316$, $p = 0.020$, Fig. 2b, c) and with dPVS counts (early-stage: $r = 0.514$, $p < 0.0001$; advanced-stage: $r = 0.271$, $p = 0.047$, Fig. 2e, f). Multivariate linear regression models, adjusted for potential confounders (age, gender, disease duration and vascular risk factors), yielded similar findings. For total PVS, early-stage $\beta = 0.407$, $p = 0.002$; advanced-stage $\beta = 0.308$, $p = 0.020$. For dPVS, early-stage $\beta = 0.526$, $p < 0.0001$; advanced-stage $\beta = 0.255$, $p = 0.047$ (Supplementary Table 1). These results indicate that the relationship between CP volume and PVS/dPVS counts is stronger in early-stage PD.

Associations between CP volume and PVS/dPVS across brain regions

Partial correlation analysis identified significant positive correlations between CP volume and PVS counts in the midbrain ($r = 0.341$, $p < 0.0001$) and basal ganglia ($r = 0.276$, $p = 0.002$) after adjusting for covariates such as age, gender, education, and vascular risk factors. A similar pattern emerged for dPVS, with significant correlations observed in the midbrain ($r = 0.285$, $p = 0.002$), basal ganglia ($r = 0.348$, $p < 0.0001$), and centrum semiovale ($r = 0.204$, $p = 0.026$). No significant correlations were found for PVS counts in the centrum semiovale (Fig. 3). Multivariate regression analysis, consistent with the partial correlation findings, yielded similar results (Supplementary Table 2). Specifically, for CP volume and PVS: midbrain $\beta = 0.341$, $p < 0.0001$; basal ganglia $\beta = 0.277$, $p = 0.002$. For CP volume and dPVS: midbrain $\beta = 0.285$, $p = 0.002$; basal ganglia $\beta = 0.341$, $p < 0.0001$; centrum semiovale $\beta = 0.203$, $p = 0.026$. These results suggest that larger CP volume correlates with impaired glymphatic clearance in specific brain regions, particularly in deep white matter.

Associations between clinical severity and MRI features

Partial correlation analysis showed that MDS-UPDRS III scores were significantly associated with CP volume ($r = 0.288$, $p = 0.002$). MDS-UPDRS III scores were also correlated with total PVS/dPVS counts and basal ganglia PVS/dPVS counts (basal ganglia PVS: $r = 0.182$, $p = 0.030$; basal ganglia dPVS: $r = 0.290$, $p = 0.001$; centrum semiovale dPVS: $r = 0.283$, $p = 0.002$). No significant correlation was observed between MDS-UPDRS III and PVS/dPVS in the midbrain. Hoehn&Yahr (H&Y) stage did not correlate with CP volume and PVS/dPVS counts (Fig. 4 and Supplementary Fig. 1).

Subsequent mediation analysis revealed that CP volume and PVS jointly influenced motor symptoms, with basal ganglia dPVS counts serving as a significant mediator in this relationship, explaining 30.52% of the total effect ($p < 0.05$, Fig. 5). While PVS/dPVS in midbrain and centrum semiovale did not show mediation effect ($p > 0.05$).

Among MDS-UPDRS III subscores, bradykinesia and rigidity scores were significantly associated with CP volume and total PVS/dPVS counts (all $p < 0.05$). Additionally, both bradykinesia and rigidity scores were significantly correlated with basal ganglia dPVS counts (bradykinesia and basal ganglia dPVS: $r = 0.272$, $p = 0.003$; rigidity and basal ganglia dPVS: $r = 0.287$, $p = 0.002$). Tremor scores and axial symptoms scores showed no significant association with basal ganglia dPVS counts (Fig. 4 and Supplementary Fig. 2).

Discussion

Our study provides novel evidence linking CP enlargement to glymphatic dysfunction and its role in motor symptom severity in PD. In contrast to previous studies primarily focused on Alzheimer's disease or cerebral small vessel disease, our research specifically examines PD patients. It highlights the spatial and temporal dynamics of CP-glymphatic interactions across different disease stages. These findings enhance our understanding of the pathophysiological mechanisms underlying PD and suggest potential targets for early intervention.

Stratified analysis revealed a stronger relationship between CP volume and glymphatic dysfunction in early-stage PD compared to advanced stages, emphasizing the dynamic nature of these interactions throughout the disease. In early-stage patients, CP volume was strongly correlated with PVS/dPVS counts in the midbrain and basal ganglia—regions essential for early α-synuclein clearance[16,17]. This suggests that CP enlargement may significantly impair glymphatic clearance during the initial stages of α-synuclein propagation, when glymphatic function is still active but increasingly burdened by accumulating protein aggregates. Interestingly, the association between CP volume and PVS/dPVS counts diminished in advanced-stage patients. A plausible explanation for this is a ceiling effect, where glymphatic dysfunction and protein aggregation reach saturation as the disease progresses, limiting further measurable associations[8,18]. Additionally, α-synuclein pathology is known to spread to cortical regions in advanced PD[19,20], potentially shifting the glymphatic burden to areas like the centrum semiovale, which we found to show no significant correlations in the early stage. These observations suggest that CP enlargement has its most pronounced impact on glymphatic clearance during early PD, highlighting a critical window for therapeutic intervention aimed at preserving glymphatic function and reducing α-synuclein accumulation.

Region-specific partial correlation analysis demonstrate that CP enlargement correlates selectively with glymphatic dysfunction across distinct brain regions. Significant associations were observed between CP volume and PVS/dPVS counts in the midbrain and basal ganglia, whereas such correlations were only present in the centrum semiovale in advanced stages. This spatial pattern likely reflects region-specific vulnerabilities in glymphatic clearance, driven by variations in anatomical structure, vascular density, and glymphatic flow dynamics[21,22]. The midbrain and basal ganglia, as early sites of α-synuclein accumulation, are particularly susceptible to glymphatic clearance impairments. This aligns with Braak's staging hypothesis, which suggests that α-synuclein pathology initially develops in the brainstem and basal ganglia before spreading to cortical regions[13,23]. Impaired glymphatic flow in these areas may exacerbate protein aggregation, creating a feedback loop of clearance dysfunction and pathological spread[11,24]. Interestingly, CP volume was not significantly correlated with the total PVS counts in the centrum semiovale but was associated with dPVS counts. This suggests that a larger CP is linked to the extent of PVS enlargement rather than an overall increase in PVS number, possibly due to CP-related glymphatic dysfunction, impaired perivascular drainage, or inflammation[25,26]. These findings indicate that spatially distinct patterns of glymphatic dysfunction closely follow the progression of α-synuclein pathology, underscoring the regional specificity of CP-glymphatic interactions in PD. Given that PD pathology typically begins in the brainstem and basal ganglia, optimizing glymphatic function in these regions could potentially slow disease progression.

Building on these region-specific findings, we further explored their clinical relevance using multivariate and mediation analyses. Only dPVS in

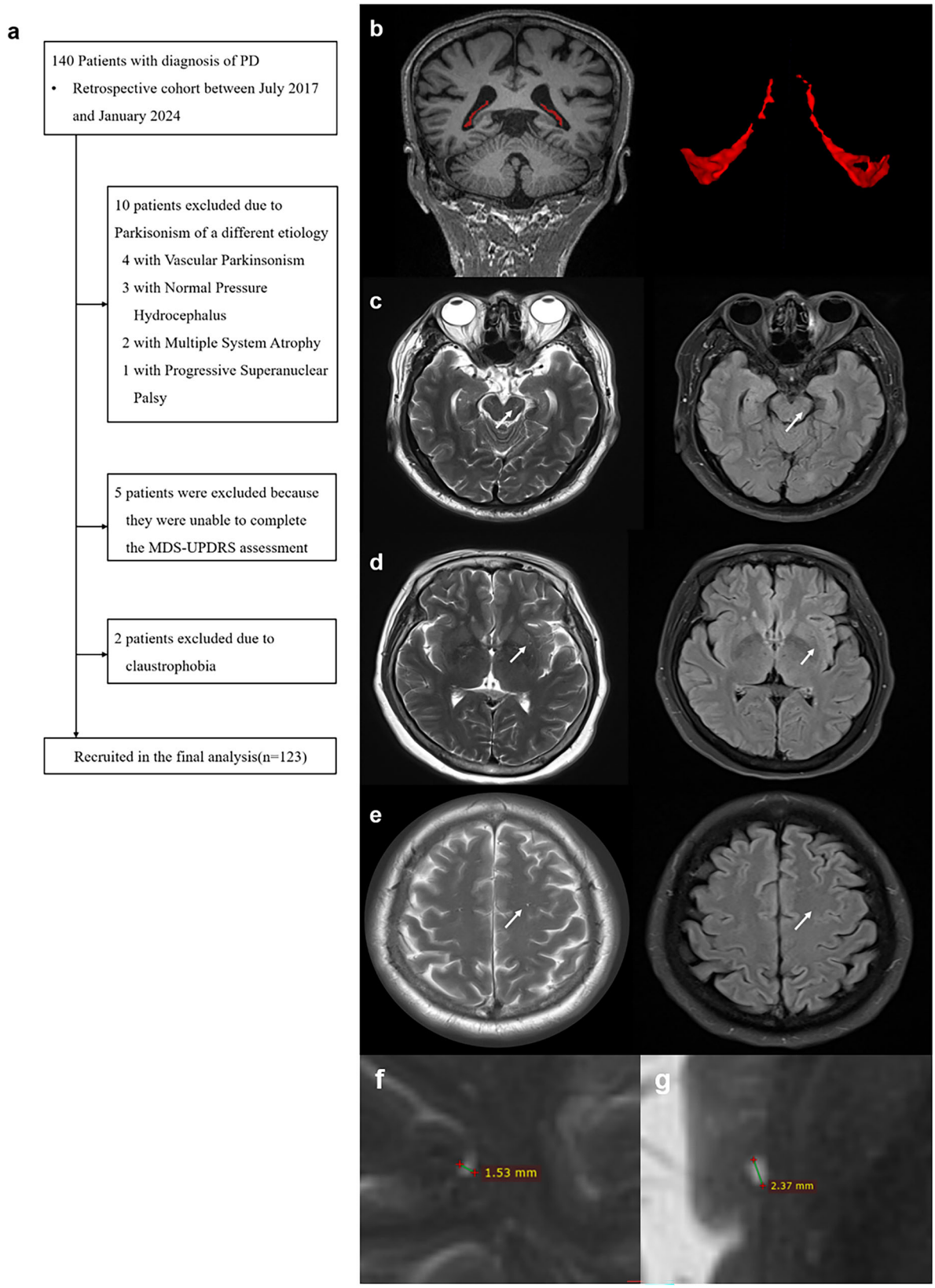

Fig. 1 | Patient enrollment and assessment process of CP and PVS. a Flowchart for patient enrollment. **b** CP volume (red) segmented from T1-weighted volumetric images via ITK-SNAP. **c**–**e** PVS readily detectable on T2-weighted and T2 FLAIR brain MRI scans. **c** PVS/dPVS in midbrain on axial MRI slices indicated by arrows. **d** PVS/dPVS in basal ganglia indicated by arrows. **e** PVS/dPVS in centrum semiovale indicated by arrows. **f** PVS with a diameter of less than 2 millimeters. **g** PVS with a diameter of ≥2 millimeters is a dPVS. FLAIR, fluid attenuated inversion recovery.

Table 1 | Demographic and MRI characteristics of patients

Characteristics	Patients with PD (n = 123)	Patients of early-stage (n = 65)	Patients of advanced-stage (n = 58)	p value
Demographic characteristics				
Age(median, range)(yr)	66(41–85)	66(45–82)	66.5(41–85)	0.368
Sex(female), no.(%)	50(40.3)	26(40.0)	24(41.4)	0.876
Education(median, range)(yr)	5(0–16)	5(0–16)	6(0–16)	0.463
Hypertension, no.(%)	44(35.5)	24(30.7)	20(34.5)	0.778
Diabetes, no.(%)	16(12.9)	10(15.4)	6(10.3)	0.407
Duration(median, range)(yr)	4(0.5–28)	2(0.5–8)	7(1–28)	<0.001
H&Y stage(median, range)	2(1–5)	2(1–2.5)	3(3–5)	<0.001
MDS-UPDRS I (median, range)	10(0–29)	9(0–22)	12(0–29)	0.002
MDS-UPDRS II (median, range)	12(0–49)	10(1–28)	15(5–49)	<0.001
MDS-UPDRS III (median, range)	42(11–75)	33(11–61)	48.5(12–75)	<0.001
MRI features				
TIV(ml) (means ± SD)	1486.07 ± 143.864	1476.91 ± 153.060	1496.33 ± 133.384	0.358
CP volume, ratio of TIV×10^3	1.10 ± 0.32	1.055 ± 0.28	1.15 ± 0.35	0.238
Number of BG-PVS	7(3–34)	7(3–25)	7(4–34)	0.248
Number of BG-dPVS	3(0–12)	3(0–9)	3(0–20)	0.218
Number of MB-PVS	3(0–12)	3(0–12)	3(0–8)	0.818
Number of MB-dPVS	1(0–7)	1(0–5)	1(0–5)	0.392
Number of CSO-PVS	0(0–10)	0(0–8)	1(0–10)	0.314
Number of CSO-dPVS	0(0–3)	0(0–6)	1(0–6)	0.362
Number of PVS	11(5–48)	11(5–35)	12(5–48)	0.163
Number of dPVS	4(0–14)	5(0–16)	5(1–22)	0.447

PD Parkinson's disease, *H&Y stage* Hoehn and Yahr stage, *MDS-UPDRS* Movement Disorder Society Unified Parkinson's Disease Rating Scale, *MRI* magnetic resonance imaging, *TIV* total intracranial volume, *CP* choroid plexus, *BG* basal ganglion, *MB* midbrain, *CSO* centrum semiovale regions, *PVS* perivascular spaces, *dPVS* dilated perivascular spaces.

the basal ganglia showed significant associations with motor severity and mediated the relationship between CP volume and MDS-UPDRS III scores, emphasizing the basal ganglia's critical role in PD. As a core node in extrapyramidal circuits, the basal ganglia integrate cortical and thalamic glutamatergic input with dopaminergic signals from the substantia nigra pars compacta to regulate voluntary movement. In contrast, the midbrain primarily provides dopaminergic input and is less directly involved in motor output, while the centrum semiovale, composed mainly of projection and association fibers, is not a key structure in motor control[27,28]. The dPVS in these regions may instead reflect nonspecific white matter changes, which could explain the absence of a mediating effect in the CP-motor severity relationship.

Symptom specific analyses further clarified the partial mediation effect. Basal ganglia dPVS were significantly associated with bradykinesia and rigidity (symptoms closely linked to basal ganglia dysfunction) but not with tremor or axial symptoms, which are thought to involve distinct neural circuits such as the thalamocortical-cerebellar and cortico-brainstem pathways[29–31]. Given that the MDS-UPDRS III includes all four symptom domains, the limited correlation of dPVS in basal ganglia with only two of them likely attenuated the overall mediation effect. These findings indicated that basal ganglia glymphatic dysfunction is selectively associated with certain motor symptoms, consistent with the clinical heterogeneity of PD. Meanwhile, MDS-UPDRS scores showed stronger correlations with MRI features than the H&Y stage scale, indicating greater sensitivity to structural brain changes linked to motor severity[32].

This study has several limitations. First, the single-center design and small sample size limit the generalizability of the findings, and larger multi-center studies are needed for validation. Second, because circadian rhythms regulate cerebrospinal fluid production, the lack of control over scanning times may have introduced variability in CP measurements. After controlling scanning time, the main findings remained consistent (data not shown). Third, the absence of a control group limits the ability to determine whether the observed MRI changes are specific to PD or reflect broader pathophysiological processes, which can be resolved through future validation studies employing the appropriate controls. Furthermore, while we used PVS/dPVS counts as markers of glymphatic dysfunction, future research should incorporate alternative imaging techniques, such as contrast-enhanced MRI and quantitative PVS volume measurements, to more comprehensively evaluate glymphatic dysfunction at different stages of PD[33,34].

In conclusion, our study demonstrates radiographic evidence linking CP enlargement to glymphatic dysfunction in PD, contributing to motor symptom severity. These findings emphasize the significance of early-stage CP and glymphatic system dysfunction in PD pathogenesis and highlight their potential as therapeutic targets. Further research is necessary to investigate these mechanisms and their implications for clinical practice.

Methods

Participants

This retrospective, cross-sectional study included 140 patients with PD admitted to the First Affiliated Hospital of Fujian Medical University between July 2017 and January 2024. Patients were identified through a systematic review of electronic medical records. All clinical and imaging assessments used in this study were conducted as part of routine diagnostic and therapeutic procedures during hospitalization. PD diagnosis was confirmed by two movement disorder specialists (each with ≥15 years of experience) based on the Movement Disorder Society clinical diagnostic criteria[35]. Motor symptom evaluations, as well as high-resolution MRI scans, were conducted during routine clinical care and retrospectively included in this study. To ensure data quality and cohort homogeneity, we excluded patients meeting the following criteria: (i) patients with atypical parkinsonism syndromes or secondary Parkinson-like symptoms caused by other

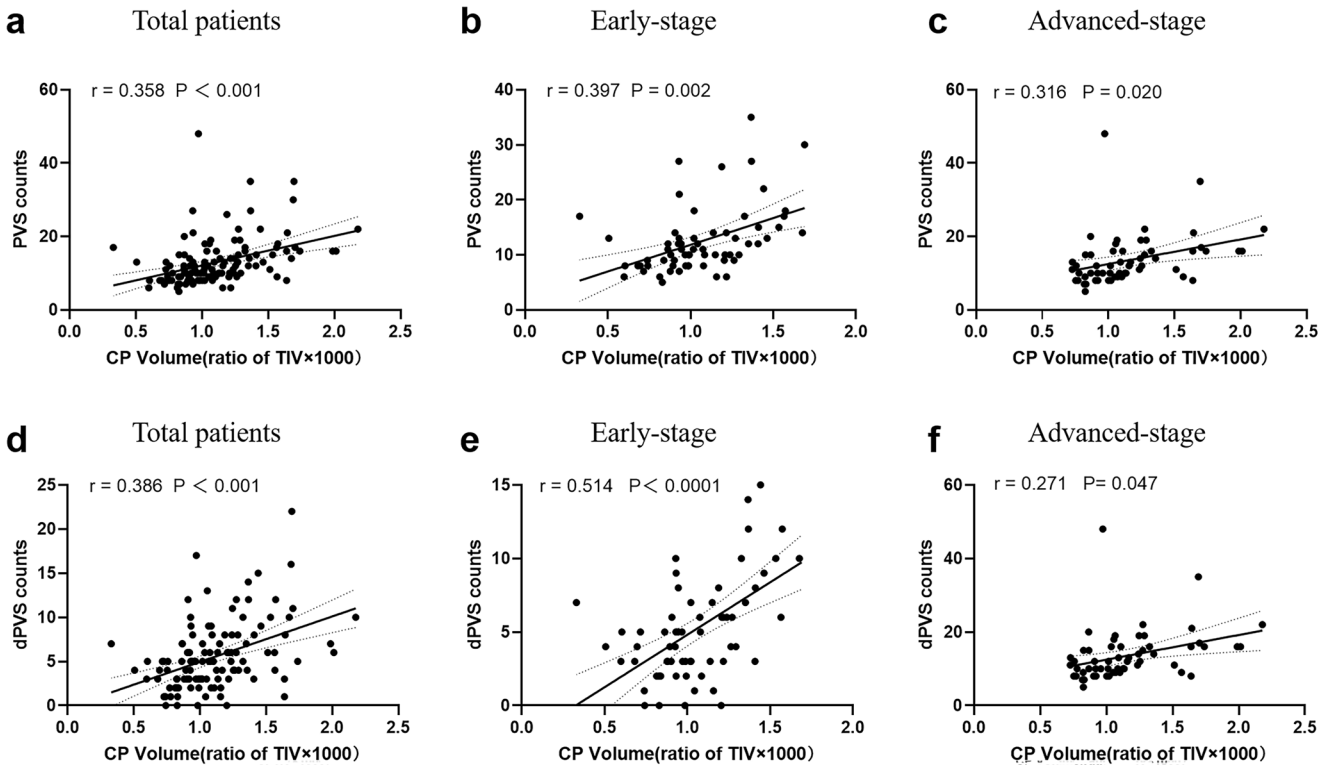

Fig. 2 | Relationship between CP volume and PVS/dPVS in 123 patients and patients in early- and advanced-stage groups. Scatterplots showing the significant association of CP volume with PVS in all patients (**a**) and those at early-stages (**b**) and advanced-stages (**c**). Association of CP volume with dPVS in all patients (**d**) and those at early-stages (**e**) and advanced-stages (**f**). Early-stages: $N = 65$; advanced-stages: $N = 58$. Statistical significance was calculated by partial correlation analysis. r-values are partial correlation coefficients after correction for age, sex, disease duration, and vascular risks. Abbreviations for different brain structures (TIV, CP, PVS, dPVS, MB, BG, CSO) were indicated in Table 1.

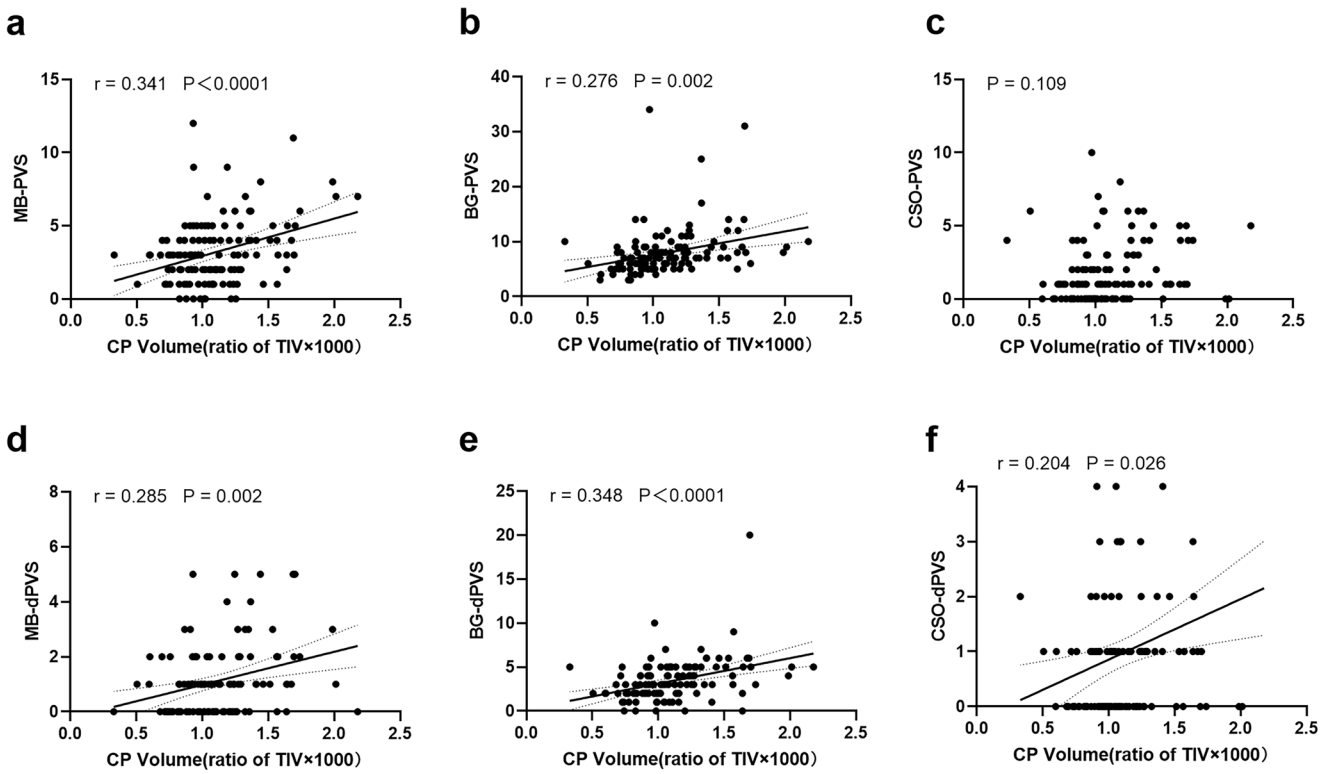

Fig. 3 | Relationship between CP volume and PVS/dPVS across brain regions in patients with PD (N = 123). Scatterplots showing association of CP volume with PVS (**a**–**c**) and dPVS (**d**–**f**). Statistical significance was calculated by partial correlation analysis. r-values are partial correlation coefficients after correction for age, sex, disease duration, and vascular risks. Abbreviations for different brain structures (TIV, CP, PVS, dPVS, MB, BG, CSO) were indicated in Table 1.

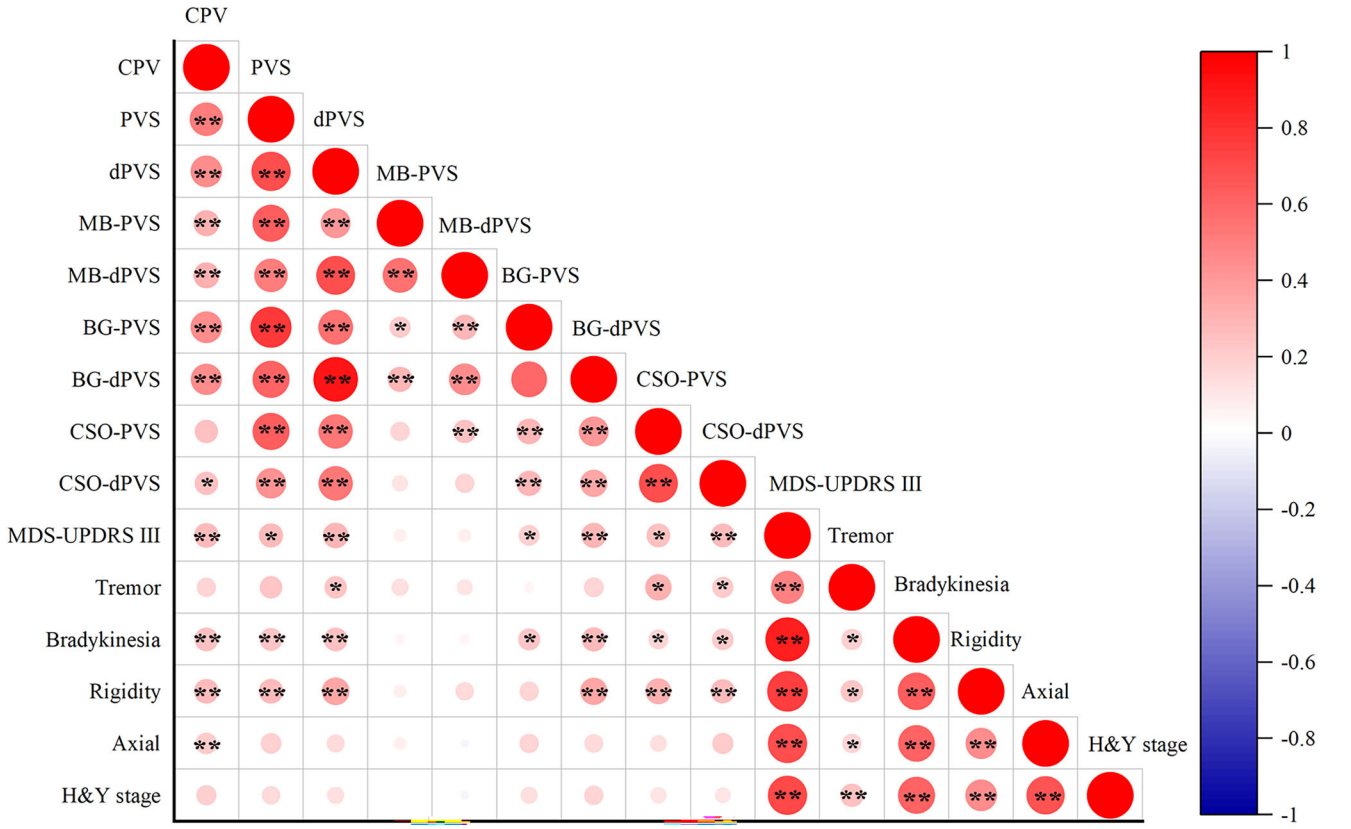

Fig. 4 | Correlation matrix of clinical scales and MRI features in 123 PD patients. The heatmap illustrates the correlation coefficients between clinical measures (H&Y stage, MDS-UPDRS III total score, and its subscores: tremor, bradykinesia, rigidity, and axial symptoms) and MRI-derived features (CP volume, total PVS/dPVS counts, and regional PVS/dPVS counts in the MB, BG and CSO. Correlations are visually represented using a color scale, with red indicating positive correlations and blue indicating negative correlations, according to the scale bar on the right. Larger circles represent stronger correlations, with statistical significance denoted by $p < 0.05$ (*) and $p < 0.01$ (**). Age, sex, disease duration and vascular risk factors were included as covariates. Abbreviations (CP, PVS, dPVS, MB, BG, CSO, MDS-UPDRS and H&Y) were indicated in Table 1.

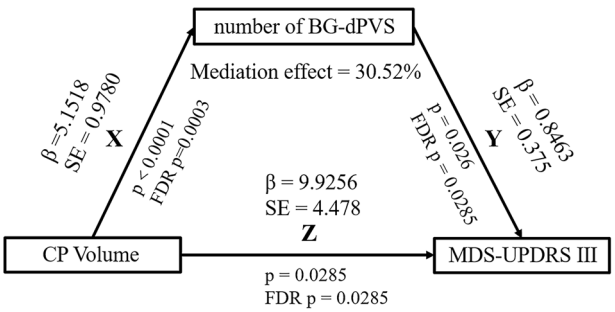

Fig. 5 | Mediation analysis of associations between CP volume, dPVS, and MDS-UPDRS III scores. Path diagram of the causal mediation model where the effect of CP volume on motor symptoms is plotted in path Z, the effect of CP volume on dPVS is plotted in path X, and the effect of dPVS on motor symptoms is plotted in path Y. Betas and p-values from regression analyses are indicated for each association. The total effect of path Z is composed of the sum of the average direct effects and the average causal mediation effect. Statistical significance was calculated by mediation analysis. The Benjamini-Hochberg method was used for multiple comparisons. Abbreviations (CP, dPVS, BG and MDS-UPDRS) were indicated in Table 1.

neurological disorders or drug effects; (ii) inability to undergo MRI due to reasons such as claustrophobia, pacemakers, or intraocular foreign bodies; (iii) poor-quality MRI images, including low spatial resolution, poor contrast, or motion artifacts; and (iv) incomplete clinical data. After applying these criteria, 123 PD patients were included in the final analysis (Fig. 1a).

This study was approved by the Institutional Ethics Review Board of the First Affiliated Hospital of Fujian Medical University (Approval No. MRCTA, ECFAH of FMU [2023]151). Written informed consent was obtained from all participants to authorize the retrospective use of their previously collected clinical records and imaging data for research purposes. All procedures complied with the ethical standards of the institutional review board and the Declaration of Helsinki and its later amendments.

Clinical evaluation

For all included participants, clinical assessment data were retrospectively obtained from medical records and included demographic information, vascular risk factors, motor symptom evaluations, and imaging findings. Disease stage was classified using the H&Y scale, and motor symptom severity was assessed using the Movement Disorder Society Unified Parkinson's Disease Rating Scale (MDS-UPDRS III). All motor assessments were performed in the "off" medication state to eliminate the influence of dopaminergic treatment. Subscores for tremor, bradykinesia, rigidity and axial symptoms were calculated from the respective subitems of the MDS-UPDRS III, as described in previous studies[36,37]. Patients were stratified into early-stage (H&Y stage ≤ 2.5) and advanced-stage (H&Y stage > 2.5) groups. This classification, widely used in previous studies, provides a reliable framework for assessing disease severity while ensuring balanced group sizes for analysis[38,39]. All clinical evaluations were conducted by experienced neurologists (≥ 15 years of expertise) following standardized protocols to ensure assessment reliability[40].

MRI acquisition and postprocessing

High-resolution MRI data were retrospectively collected from routine clinical scans performed using a 3-T Skyra Siemens scanner (Siemens, Munich, Germany). All scans had been acquired during standard diagnostic procedures, with patients in the supine position and head immobilized using foam pads to reduce motion artifacts. Consistent imaging parameters were used across patients in clinical practice, including: for 3D T1-weighted imaging, a repetition time of 2,300 ms, echo time of 2.32 ms, flip angle of 8°, field of view (FOV) = 240 × 240 mm², slice thickness = 0.9 mm, matrix size = 256 × 256, and 192 slices; and for T2 FLAIR imaging, repetition time = 8,500 ms, echo time = 81 ms, FOV = 200 × 220 mm², matrix size = 224 × 320, inversion time = 2,440 ms, and slice thickness = 5.0 mm with a 1.0 mm interslice gap[41].

For morphometric analysis, we processed 3D-T1 images using the Computational Anatomy Toolbox (CAT12, Jena University Hospital) within the Statistical Parametric Mapping (SPM12) package, running in MATLAB R2021a (MathWorks, Natick, MA, USA). We applied the default processing pipeline, which included bias correction for field inhomogeneities, segmentation into gray matter, white matter, and CSF, and normalization using DARTEL. We calculated the total intracranial volume (TIV) as the sum of total gray matter, white matter, and CSF volumes to represent head size.

The CP in the lateral ventricles was manually segmented by two trained neuroradiologists. A third neuroradiologist systematically quality-checked the segmentation. We performed the segmentation in the sagittal, axial, and coronal planes of the 3D T1-weighted magnetization-prepared rapid gradient-echo (MPRAGE) scans using ITK-SNAP software (version 3.8.0; http://www.itksnap.org/), and calculated the CP volume. Manual segmentation was chosen for CP volume measurement due to its superior accuracy in delineating small, anatomically complex structures compared to automated methods[42]. Figure 1b illustrates the segmentation and volume calculation process. We expressed regional volume as a ratio to TIV to account for individual differences in head size. The intraclass correlation coefficient (ICC) between the two neuroradiologists showed excellent agreement (ICC = 0.92) for CP measurements. All three neuroradiologists were blinded to the clinical and other imaging data of the patients. We excluded CP measurements from the third and fourth ventricles due to inconsistent visualization on the 3D-T1 images, which made precise segmentation difficult.

PVS exhibit signal intensities similar to cerebrospinal fluid across all imaging sequences. They typically align with perforating arteries and appear round or ovoid, with diameters less than 3 mm. PVS are most commonly located in the inferior basal ganglia, centrum semiovale, and midbrain, and lack a surrounding gliotic rim, distinguishing them from lacunes[25]. We quantified PVS with diameters of ≥ 2 mm (referred to as "dPVS") by measuring the widest diameter on coronally reformatted T1 slices. The 2 mm threshold was based on previous studies of PVS[43,44].

We calculated the number of PVS and dPVS from axial T2-weighted images using an open-source DICOM viewer (RadiAnt, Medixant, Poland). Two neuroradiologists, who were blinded to the participants' diagnoses and clinical details, performed the measurements. T2-weighted FLAIR images were consulted to differentiate PVS from lacunar infarcts (Fig. 1c–g). Consistent with prior research, we quantified PVS in the slice containing the maximum number of PVS within the basal ganglia, midbrain, and centrum semiovale regions[45,46]. The interrater reliability was excellent, with an ICC of 0.90, and any discrepancies were resolved through consensus.

Statistical analyses

Statistical analysis was conducted using SPSS Statistics (Version 26, IBM Corporation, Armonk, NY, USA), GraphPad Prism software (Version 9, GraphPad Software, San Diego, CA, USA), Origin Software (Version 2024, OriginLab Corporation, Northampton, Massachusetts, USA) and R software (Version 4.3.3, http://www.r-project.org). Continuous variables are presented as medians with ranges, while categorical variables are expressed as percentages.

Step 1: Stage-specific associations between CP Volume and PVS/dPVS: Partial correlation and multivariate linear regression analyses was performed between CP volume and PVS/dPVS counts in early- and advanced stages. A two-tailed p value of <0.05 was considered significant. For the regression analyses, we tested model assumptions, including linearity, multicollinearity (variance inflation factor [VIF] < 10), and residual normality (Shapiro-Wilk test). Model fit was assessed using adjusted R^2, with $p < 0.05$ considered statistically significant. Age, sex, disease duration and vascular risk factors (hypertension or diabetes) were included as covariates due to their potential influence.

Step 2: Association between CP volume and PVS/dPVS across brain regions: Partial correlation and multivariate linear regression analyses was performed between CP volume and PVS/dPVS counts in the midbrain, basal ganglia and centrum semiovale. Age, sex, disease duration and vascular risk factors were included as covariates. A two-tailed p value of <0.05 was considered significant.

Step 3: Relationship between MRI features and clinical scores: Partial correlation analyses was performed between MRI features (CP volume, total PVS/dPVS counts and PVS/dPVS counts in the midbrain, basal ganglia and centrum semiovale), and clinical scores (MDS-UPDRS III and subscores). Age, sex, disease duration and vascular risk factors were included as covariates. A two-tailed p value of <0.05 was considered significant. Relationship among CP volume, PVS/dPVS counts, and PD symptoms: To explore potential mediation effects, we applied a simple mediation model ("model 4" in PROCESS for SPSS), with CP volume as the independent variable (IV), motor symptom severity (MDS-UPDRS III) as the dependent variable (DV), and PVS metrics as the mediator (M). We used bootstrapping with 5,000 resamples to estimate the indirect effects and their confidence intervals. A significant mediation effect was identified when the bootstrapped confidence intervals for the indirect effect did not include zero. The Benjamini-Hochberg (FDR) method was applied for multiple comparison.

Data availability

The data that support the findings of this study are available on request from the corresponding author. The data are not publicly available, as it contain information that could compromise the privacy of study participants.

Received: 8 January 2025; Accepted: 19 April 2025;
Published online: 22 May 2025

References

1. Morris, H. R., Spillantini, M. G., Sue, C. M. & Williams-Gray, C. H. The pathogenesis of Parkinson's disease. *Lancet***403**, 293–304 (2024).
2. Ben-Shlomo, Y. et al. The epidemiology of Parkinson's disease. *Lancet***403**, 283–292 (2024).
3. Boland, B. et al. Promoting the clearance of neurotoxic proteins in neurodegenerative disorders of ageing. *Nat. Rev. Drug Discov.* **17**, 660–688 (2018).
4. Rasmussen, M. K., Mestre, H. & Nedergaard, M. Fluid transport in the brain. *Physiol. Rev.* **102**, 1025–1151 (2022).
5. Christensen, J., Li, C. & Mychasiuk, R. Choroid plexus function in neurological homeostasis and disorders: the awakening of the circadian clocks and orexins. *J. Cereb. Blood Flow Metab.***42**, 1163–1175 (2022).
6. Xie, L. et al. Sleep drives metabolite clearance from the adult brain. *Science* **342**, 373–377 (2013).
7. Sládek, M. et al. The circadian clock in the choroid plexus drives rhythms in multiple cellular processes under the control of the suprachiasmatic nucleus. *Fluids Barriers CNS* **21**, 46 (2024).
8. Jeong, S. H. et al. Choroid plexus volume, amyloid burden, and cognition in the Alzheimer's disease continuum. *Aging Dis.* https://doi.org/10.14336/ad.2024.0118 (2024).
9. Vandendriessche, C. et al. The spreading and effects of human recombinant α-synuclein preformed fibrils in the cerebrospinal fluid of mice. *eNeuro* **11**, https://doi.org/10.1523/eneuro.0024-23.2024 (2024).
10. Jeong, S. H. et al. Association of choroid plexus volume with motor symptoms and dopaminergic degeneration in Parkinson's disease. *J. Neurol. Neurosurg. Psychiatry* **94**, 1047–1055 (2023).

11. Chung, S. J. et al. Perivascular spaces in the basal ganglia and long-term motor prognosis in newly diagnosed Parkinson disease. *Neurology* **96**, e2121–e2131 (2021).
12. Lv, W. et al. Normal-sized basal ganglia perivascular space related to motor phenotype in Parkinson freezers. *Aging***13**, 18912–18923 (2021).
13. Braak, H. et al. Staging of brain pathology related to sporadic Parkinson's disease. *Neurobiol. Aging* **24**, 197–211 (2003).
14. Cui, H. et al. Decreased AQP4 expression aggravates α-synuclein pathology in Parkinson's disease mice, possibly via impaired glymphatic clearance. *J. Mol. Neurosci.* **71**, 2500–2513 (2021).
15. Bohnen, N. I. & Hu, M. T. M. Sleep disturbance as potential risk and progression factor for Parkinson's disease. *J. Parkinsons Dis.* **9**, 603–614 (2019).
16. Henderson, M. X. et al. The roles of connectivity and neuronal phenotype in determining the pattern of α-synuclein pathology in Parkinson's disease. *Neurobiol. Dis.* **168**, 105687 (2022).
17. Fares, M. B., Jagannath, S. & Lashuel, H. A. Reverse engineering Lewy bodies: how far have we come and how far can we go?. *Nat. Rev. Neurosci.* **22**, 111–131 (2021).
18. Bjorkli, C., Sandvig, A. & Sandvig, I. Bridging the gap between fluid biomarkers for Alzheimer's disease, model systems, and patients. *Front. Aging Neurosci.* **12**, 272 (2020).
19. Nedergaard, M. & Goldman, S. A. Glymphatic failure as a final common pathway to dementia. *Science* **370**, 50–56 (2020).
20. Braak, H., Rüb, U., Schultz, C. & Del Tredici, K. Vulnerability of cortical neurons to Alzheimer's and Parkinson's diseases. *J. Alzheimers Dis.* **9**, 35–44 (2006).
21. Kress, B. T. et al. Impairment of paravascular clearance pathways in the aging brain. *Ann. Neurol.* **76**, 845–861 (2014).
22. Wardlaw, J. M. et al. Perivascular spaces in the brain: anatomy, physiology and pathology. *Nat. Rev. Neurol.* **16**, 137–153 (2020).
23. Braak, H., Ghebremedhin, E., Rüb, U., Bratzke, H. & Del Tredici, K. Stages in the development of Parkinson's disease-related pathology. *Cell Tissue Res.* **318**, 121–134 (2004).
24. Zhang, Y. et al. Interaction between the glymphatic system and α-synuclein in Parkinson's disease. *Mol. Neurobiol.* **60**, 2209–2222 (2023).
25. Ramirez, J. et al. Small and large magnetic resonance imaging-visible perivascular spaces in the basal ganglia of Parkinson's disease patients. *Mov. Disord.***37**, 1304–1309 (2022).
26. Cai, Y. et al. The relationship between inflammation, impaired glymphatic system, and neurodegenerative disorders: a vicious cycle. *Neurobiol. Dis.* **192**, 106426 (2024).
27. McGregor, M. M. & Nelson, A. B. Circuit mechanisms of Parkinson's disease. *Neuron* **101**, 1042–1056 (2019).
28. Li, R. et al. Basal ganglia atrophy-associated causal structural network degeneration in Parkinson's disease. *Hum. Brain Mapp.* **43**, 1145–1156 (2022).
29. Herb, J. N. et al. Cortical implications of advancing age and disease duration in Parkinson's disease patients with postural instability and gait dysfunction. *J. Parkinsons Dis.* **6**, 441–451 (2016).
30. Zhang, J. R., Feng, T., Hou, Y. N., Chan, P. & Wu, T. Functional connectivity of vim nucleus in tremor- and akinetic-/rigid-dominant Parkinson's disease. *CNS Neurosci. Ther.***22**, 378–386 (2016).
31. Piccinin, C. C. et al. Differential pattern of cerebellar atrophy in tremor-predominant and akinetic/rigidity-predominant Parkinson's disease. *Cerebellum***16**, 623–628 (2017).
32. Kawasaki, T. et al. Motor planning error in Parkinson's disease and its clinical correlates. *PLoS ONE* **13**, e0202228 (2018).
33. He, P. et al. The association of the glymphatic function with Parkinson's disease symptoms: neuroimaging evidence from longitudinal and cross-sectional studies. *Ann. Neurol.* **94**, 672–683 (2023).
34. Yamamoto, E. A. et al. The perivascular space is a conduit for cerebrospinal fluid flow in humans: a proof-of-principle report. *Proc. Natl Acad. Sci. USA* **121**, e2407246121 (2024).
35. Postuma, R. B. et al. MDS clinical diagnostic criteria for Parkinson's disease. *Mov. Disord.***30**, 1591–1601 (2015).
36. Zampogna, A. et al. Axial impairment and falls in Parkinson's disease: 15 years of subthalamic deep brain stimulation. *NPJ Parkinsons Dis.* **8**, 121 (2022).
37. Martínez-Fernández, R. et al. Prospective long-term follow-up of focused ultrasound unilateral subthalamotomy for Parkinson disease. *Neurology* **100**, e1395–e1405 (2023).
38. Goetz, C. G. et al. The Unified Parkinson's Disease Rating Scale (UPDRS): status and recommendations. *Mov. Dis*. **18**, 738–750 (2003).
39. Ding, X. B. et al. Impaired meningeal lymphatic drainage in patients with idiopathic Parkinson's disease. *Nat. Med.* **27**, 411–418 (2021).
40. Liu, W. et al. Vision-based estimation of MDS-UPDRS scores for quantifying Parkinson's disease tremor severity. *Med. Image Anal.* **85**, 102754 (2023).
41. Lin, Y. et al. Six visual rating scales as a biomarker for monitoring atrophied brain volume in Parkinson's disease. *Aging Dis.* **11**, 1082–1090 (2020).
42. Choi, J. D. et al. Choroid plexus volume and permeability at brain MRI within the Alzheimer disease clinical spectrum. *Radiology* **304**, 635–645 (2022).
43. Rudie, J. D., Rauschecker, A. M., Nabavizadeh, S. A. & Mohan, S. Neuroimaging of dilated perivascular spaces: from benign and pathologic causes to mimics. *J. Neuroimaging* **28**, 139–149 (2018).
44. Favaretto, A. et al. Enlarged Virchow Robin spaces associate with cognitive decline in multiple sclerosis. *PLoS ONE* **12**, e0185626 (2017).
45. Kim, S. et al. Regional burden of enlarged perivascular spaces and cognition and neuropsychiatric symptoms in drug-naive patients with Parkinson disease. *Neurology* **102**, e209483 (2024).
46. Ineichen, B. V. et al. Dilated Virchow-Robin spaces are a marker for arterial disease in multiple sclerosis. *EBioMedicine* **92**, 104631 (2023).

Acknowledgements

We thank the patients for granting permission to publish this information. This research was supported by the National Natural Science Foundation of China (82371253), the Natural Science Foundation of Fujian Province under Grant (2024Y4017) and the National Natural Science Foundation of China (82301698).

Author contributions

L.L., Q.W., Q.C. and X.Y. contributed equally to this work and those are considered first authors. N.W., X.L. and Y.L. conceptualized and designed the study. L.L., Q.W., Q.C., Y.S. and X.Y. acquired the data. L.L., Q.W., Q.C., W.H., H.L. and Y.Z. analyzed and interpreted the data. Q.W., Y.S., J.H., M.L. and G.C. analyzed the imaging data. S.X. performed the statistical analysis. L.L., Q.W., Q.C. and W.H. drafted the manuscript. L.L., X.Y., X.L. and Y.L. revised draft of the manuscript. W.H. and Y.L. received the funding. Y.F. and N.W. supervised the study. All authors read and approved the final manuscript.

Competing interests

The authors declare no competing interests.

Additional information

Supplementary information The online version contains supplementary material available at https://doi.org/10.1038/s41531-025-00971-8.

Correspondence and requests for materials should be addressed to Ning Wang, Xiang Lin, Ying Fu or Yu Lin.